Two-scale Moving Boundary Dynamics of Cancer Invasion

Shuttleworth, Robyn; Trucu, Dumitru

Published in:
Cell Movement

DOI:
10.1007/978-3-319-96842-1

Publication date:
2018

Document Version
Peer reviewed version

Author Accepted Manuscript Version of Shuttleworth, R & Trucu, D 2018, Two-scale Moving Boundary Dynamics of Cancer Invasion: Heterotypic Cell Populations Evolution in Heterogeneous ECM. in M Stolarska & N Tarfulea (eds), Cell Movement: Modeling and Applications. 1 edn, Modeling and Simulation in Science, Engineering and Technology, Springer , pp. 1-24. https://doi.org/10.1007/978-3-319-96842-1

Two-scale Moving Boundary Dynamics of Cancer Invasion: Heterotypic Cell Populations Evolution in Heterogeneous ECM

Robyn Shuttleworth and Dumitru Trucu

Abstract Cancer cell invasion, recognised as one of the hallmarks of cancer, is a complex process involving the secretion of matrix-degrading enzymes that have the ability to degrade the surrounding extracellular matrix (ECM). Combined with cell proliferation and migration, and changes in cell-cell and cell-matrix adhesion, the tumour is able to spread into the surrounding tissue. The multiscale character of this process is highlighted here through the double feedback link between the cell-scale molecular processes and those occurring at the tissue level. In this chapter, we build on the multiscale moving boundary framework proposed in [30] by developing the modelling of the tissue-scale dynamics to include cell-cell and cell-matrix adhesion in a heterogeneous cancer cell population. To that end, we consider here two cancer cell sub-populations, namely a primary tumour cell distribution and a second cancer cell sub-population that arises due to mutations from the primary tumour cells and exhibits higher malignancy. We explore the multiscale moving boundary dynamics of this heterogeneous tumour cell population in the presence of cell-adhesion at the tissue-scale and matrix degrading enzyme molecular processes considered at cell-scale. Using computational simulations we examine the effect of different levels of adhesion and matrix remodelling on the invasion of cancer cells.

Robyn Shuttleworth

Division of Mathematics, University of Dundee, Scotland, DD1 4HN, e-mail: r.shuttleworth@dundee.ac.uk

Dumitru Trucu

Division of Mathematics, University of Dundee, Scotland, DD1 4HN, e-mail: trucu@maths.dundee.ac.uk

1 Introduction

Cancer invasion of tissue is a complicated, multiscale process which plays an essential role in tumour progression. Through a combination of adhesion, secretion of various matrix degrading enzymes, right from the early stages, cancer cells acquire the ability to spread locally and invade the surrounding tissue, this is further exacerbated by later secretion of growth factors that lead to the angiogenesis process that paves the way for metastatic spread, leading to the creation of secondary tumours at different locations in the human body [17]. These new colonies are known as metastases, or secondary tumours, and are the cause of 90% of human cancer deaths [10]. The most common site for breast cancer metastasis, for example, is the bone; followed by the liver and lungs [32]. Once a tumour has invaded the bone or any of these other vital organs, it is fatal and cannot be cured, only treated by various forms of cancer therapy such as surgical intervention, chemotherapy and radiation [29].

1.1 Biological Background

Recognised as one of the hallmarks of cancer [17], cancer invasion is a key process in tumour development that uses a combination of cell-cell and cell-matrix adhesion, alongside the secretion of proteolytic enzymes to degrade the surrounding tissue and this way expand on the affected area. This enables the cells at the invasive edge of the tumour to colonise new, initially healthy regions of the peritumoural tissue, where in the first instance there is no restriction in nutrients or changes in tissue structure. The ultimate success of invasion relies heavily on the capabilities of the other hallmarks of cancer [17], namely: the ability to sustain proliferative signalling, to evade growth suppressors, to enable limitless replicative potential, to induce angiogenesis and the ability to resist cell death. After a decade of further research on cancer, a wider understanding of its processes sparked the addition of another four hallmarks [18] to the original six, namely: the ability to avoid immune destruction, to deregulate cellular energetics, tumour-promoting inflammation, along with genetic instability and mutation.

A malignant tumour is comprised of a complex community of cells (fibroblasts, endothelial cells, stromal cells), all of which are mixed in with the extra-cellular matrix (ECM). The extra-cellular

matrix is a key biologically structure that provides not only support to surrounding cells and tissues [21], but also acts as a framework in which the cells can communicate and exercise spatial movement. The formation of the ECM is an essential process, particularly in wound healing and tumour invasion. The ECM is comprised of a variety of secreted proteins which can vary depending on the type of tissue or the location in which we are investigating. Such components include: collagen fibres and elastin which provide necessary structure and elasticity of the ECM, glycoprotiens such as fibronectin, laminins, and proteogylcans which bind to the collagens and to receptors on the cell surface.

Cells bind to the ECM through cell-matrix adhesion [23]. This process is regulated by a family of specific molecules on the cell surface known as cell adhesion molecules (CAM) that enable the binding process to various ECM components. These give rise to conditions in which the tumour microenvironment contributes towards cell migration within the surrounding tissue. The migratory character of the invading cells is further strengthened through the loss of cell-cell adhesion that causes these particular tumour cells to become even more motile and spread further in the tissue [9]. An important role in cell-cell adhesion is played by the cell-cell signalling pathways based on the interactions between the distribution of calcium-sensing receptors and Ca^{2+} ions from the extracellular matrix [20]. In normal, healthy cells, this calcium-dependent cell-cell adhesion process is mediated by a large family of transmembrane glycoproteins known as cadherins. Cadherins are split into many groups; the most relevant being known as E-cadherins. In order for normal cellular adhesion to take place, E-cadherin will form binds with proteins found inside the cell known as catenins, most typically the β-catenin, forming an E-cadherin/catenin complex. Any alteration to the function of β-catenin will result in the loss of ability of the E-cadherin to initiate cell-cell adhesion [33]. The direct correlation between this calcium-based cell signalling mechanism and the regulation of E-cadherin and β-catenin was first discovered in colon carcinoma [7]. This loss of cell-cell adhesion paired with a quick spread of the cells due to enhanced cell-matrix adhesion [6] enables these cancerous cells to invade the surrounding tissue [12].

Finally, a key player in the invasion process is the over-production and secretion of proteolytic enzymes. These enzymes can be categorised as matrix-degrading enzymes (MDEs) with such sub-groups as matrix metalloproteinases (MMPs) [26] and the urokinase-type plasminogen activator (uPA). The interaction of these enzymes with the ECM components results in the degradation and remodelling of the ECM. MDEs have the ability to open migratory pathways and alter cell-

cell and cell-matrix adhesion properties. One of the first MMPs to interact with the ECM is the membrane-tethered MT1-MMP. Once in the stroma, MT1-MMP will begin to cleave collagen type I into smaller pieces. As well as cleaving, MT1-MMP has another role in that it can activate pro-MMP-2. Molecules of pro-MMP-2 present in the extra-cellular matrix are recruited by the cancer cells and cleaved by MT1-MMP to promote MMP-2 activation. Once activated, MMP-2 is then available to breakdown the previously cleaved smaller pieces of collagen type I, as well as degrade the surrounding fibres in order to create a path in which the cancer cells can advance.

1.2 Mathematical Models of Cancer Invasion

The past few decades have witnessed great interest in the mathematical modelling of cancer invasion [5, 8, 11, 35]. There are many models which investigate different aspects of cancer invasion, particularly using *in vitro* models, however the *in vivo* process is much more complicated and less understood. *In vivo* models capture the complexity of tumour spread, however it is very difficult to visualise the individual steps of invasion. On the other hand, *in vitro* models are easier to construct and they allow us to control a lot of the experimental values we obtain and this allows for easier quantitative analysis. One disadvantage to *in vitro* models however is the inability to see the global effect of invasion, i.e., *in vitro* models only contain a partial expression of the interactions between the cancer cells and the ECM [22]. Great effort has been made to understand the interactions that are occurring during the invasion process, and the experiments, both *in vivo* and *in vitro* have helped to advance this knowledge. Links between cell migration processes and MMPs that are produced by the cancer cells have been discovered [24], as well as links between cell migration and the structure of the extracellular matrix [34]. There has been many attempts to model these interactions, using both continuum and discrete models, however these are "one-scale" based models, and do not consider the overall aspects of a multiscale invasion model.

The model proposed in [3] describes the invasion of tissue by cancer cells whilst considering the tumour cells, tissue (extracellular matrix) and matrix-degrading enzymes. There are two models proposed, the first a continuum model which considers the tumour mass as a whole, and a second individual-based model to investigate the invasive effects on the level of individual cells. The continuum model here describes how the tumour cells respond to haptotactic effects produced within

the ECM. It has been shown that the tumour cells will split into two groups, one driven by random migration, and the other spurred by haptotaxis. The individual-cell based model confirms this and it is concluded that haptotaxis is important for cancer cell invasion.

The first continuum approach for modelling cell-cell adhesion was proposed in [4] which considers the directed movement of cells in response to the adhesive forces made through binding. The PDE model in [3] was used as a basis for the models in [16] where a continuum model of cancer cell invasion was derived which accounts for both cell-cell and cell-matrix adhesion. These models used non-local terms for both cell-cell and cell-matrix adhesion and they introduced the notion of adhesive flux and cell sensing radius, which was to detect the immediate spatial environment. Analytical results of these models were proved by [12] using a system of nonlinear, non-local partial integro-differential equations describing the spatio-temporal dynamics of cancer invasion. The behaviours of cancer cells under different adhesion coefficients were stated.

A model describing the mesenchymal motion of cells in a fibre network was developed by [19]. Mesenchymal migration involves significant matrix remodelling, where the cell will leave a trail of aligned fibres along its path. Both mesoscopic (individual based) and macroscopic (population based) models were described and these both form a good foundation for modelling on hetereogenous orientated environments. This approach was continued by [25] using an individual-cell based model where two different forms of cell migration were investigated. Here it is shown that in terms of mesenchymal migration, the actions of both contact-guidance and ECM remodelling are sufficient processes for invasion to occur.

All of these models have been proposed at a single scale level and not do not incorporate a multiscale approach. Multiscale modelling of cancer invasion has only recently become an area of interest, where the first instance can be seen in [2]. Here, three scales were identified; extracellular, cellular and subcellular, and the effect of the microenvironment on tumour development was explored. It is shown how the three different biological scales can overlap and work together to form a more concise model of tumour invasion. Multiscale modelling was then utilised in [28] where focus lay on the interactions between E-cadherin and β-catenin and how cell migration may control cell adhesion was investigated. Both intracellular and extracellular dynamics were considered, with the conclusion that the tumour cells themselves are facilitating progression.

More recently, a multiscale moving boundary method of tumour invasion was proposed in [30] using three scale modelling; macroscale occurring at the tissue level, microscale occurring at a cellular

level and a naturally arising third scale which is used to characterise the invasive boundary of the tumour. We propose a model which builds on this original framework [30] in order to incorporate the adhesive nature of cancer cells [15] with both themselves and the surrounding microenvironment. This multiscale modelling will focus on exploring the evolution of tumour morphology whose importance is justified by clinical considerations, namely that it is not necessarily the overall size but the morphology of the tumour that creates huge surgical challenges. This is mainly due to the deficiencies in all current imaging techniques, which are only able to capture between 65% and 90% of the tumour, enabling the real possibility of not resecting the true extent of the tumour during the surgical process by leaving behind small but complicated leading-edge tumour morphological patterns that are not captured by the imaging, which subsequently lead to an aggressive tumour relapse.

2 The Multiscale Modelling Approach

We will now briefly describe the multiscale framework initially introduced in [30] for modelling cancer cell invasion and then develop the macroscopic dynamics incorporating cell-adhesion. Cancer invasion occurs at many spatial and temporal scales. The multiscale framework introduced in [30] was developed to consider detailed interactions taking place at the cellular- and tissue-scales alongside the linking between these different scales.

Within a maximal environmental tissue cube Y, at initial time t_0, $\Omega(t_0)$ represents the snapshot of the tumour domain where the combined distributions of cancer cells $c_1(t,x)$ and $c_2(t,x)$ exercise their dynamics, with c_1 and c_2 representing the sub-populations 1 (primary tumour cells) and 2 (representing mutated cells), and their combined vector being denoted by $\mathbf{c}(t,x) = [c_1(t,x), c_2(t,x)]$ (as illustrated in Figure 1). The tumour cell population exercise their activity within a supporting density of ECM that is denoted here with $v(t,x)$, and for compact notation, we will consider the combined vector of cancer cells, $\mathbf{c}$ and ECM, v, defined as

$$\mathbf{u}(t,x) := (\mathbf{c}(t,x)^T, v(t,x))^T.$$

The spatial considerations play an important role in this model. We assume that the concentration of MDEs occupy a negligible amount of space within the tissue scale tumour, and similar to

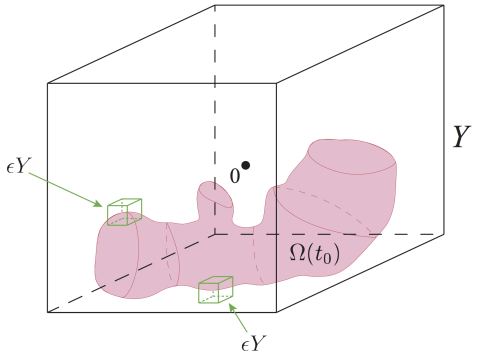

Fig. 1: *Schematic diagram showing the spatial cubic region Y centred at the origin in $\mathbb{R}^3$. The solid green lines represent the family of macroscopic ϵY cubes placed on the boundary of the tumour $\partial\Omega(t_0)$, and the pale pink region represents the initial mass of cancer cells $\Omega(t_0)$.*

the approach in [15], we shall define the *volume fraction of occupied space* as

$$\rho(t,x) \equiv \rho(\mathbf{u}(t,x)) := \vartheta_v v(t,x) + \vartheta_c \sum_{n=1}^{2} c_n(t,x)$$

where ϑ_v represents the fraction of physical space occupied by the ECM and ϑ_c is the fraction of physical space occupied by c_n.

However, while for the purpose of this work, at the tissue scales (macro-scale) we consider only cancer cells and ECM, the crucial activity of the MDEs and their dynamics is described at cell-scale (micro-scale) by accounting for spatial dynamics of proteolytic processes that occur along the invasive edge of the tumour.

2.1 Macro-scale Dynanamics

The dynamics of the two cell populations are similar in flavour. In the presence of a logistic proliferation law, per unit time, the primary tumour cells $c_1(t,x)$ are assumed to exercise spatial movement that is a combined effect of local brownian movement (approximated here through diffusion) and cell adhesion, and lose some of the cell population through certain level of mutation towards a second more motile and agressive population $c_2(t,x)$. Once mutations have started occurring, under the presence of a logistic proliferation law, population c_2 begin its own dynamics, and so per

unit time, this is also experiencing a spatial redistribution dictated by a local brownian movement (approximated again through diffusion) and cell adhesion. Therefore, mathematically, the dynamics can be re-casted as

$$\begin{aligned} \tfrac{\partial c_1}{\partial t} &= \nabla \cdot [D_1 \nabla c_1 - c_1 \mathcal{A}_1(t, x, \mathbf{u}(t, \cdot))] + \mu_1 c_1 (1 - \rho(\mathbf{u})) - M_1(t, \mathbf{u}) c_1, \\ \tfrac{\partial c_2}{\partial t} &= \nabla \cdot [D_2 \nabla c_2 - c_2 \mathcal{A}_2(t, x, \mathbf{u}(t, \cdot))] + \mu_2 c_2 (1 - \rho(\mathbf{u})) + M_1(t, \mathbf{u}) c_1. \end{aligned} \tag{1}$$

where: D_n, $n = 1, 2$ are the non-negative diffusion coefficients; $\mathcal{A}_n(t, x, \mathbf{u}(t, \cdot))$ is the non-local term accounting for cell adhesion incorporating both cell-cell and cell-matrix adhesion; μ_n describes the proliferation coefficient, here; and M_1 the final term describes the mutation from $c_1(t, x)$. To account for the physical space available and avoid overcrowding, we adopt here the proliferation term $1 - \rho(\mathbf{u})$ introduced in [16]. Furthermore, the non-local term $\mathcal{A}_n(t, x, \mathbf{u}(t, \cdot))$, known as the adhesive flux, has a form of the type proposed in [15, 16], and is given as

$$\mathcal{A}_n(t, x, \mathbf{u}(t, \cdot)) = \frac{1}{R} \int\limits_{\mathbf{B}(0,R)} \mathbf{n}(y) \cdot \mathcal{K}(||y||_2) \cdot g_n(t, \mathbf{u}(t, x + y)) \chi_{\Omega(t)}(x + y)\, dy, \quad n = 1, 2. \tag{2}$$

This describes the motion of cells due to both cell-cell and cell matrix adhesion, which occurs as a result of the forces produced when adhesion bonds are both produced and broken. Here $R > 0$ is the *sensing radius* of cell-cell and cell matrix interations, $\mathbf{B}(0, R) \subset \mathbb{R}^2$ denotes the usual ball centred at zero and of radius R, and $\chi_{\Omega(t)}(\cdot)$ represents the characteristic function of $\Omega(t)$. At any time instance t, for any $x \in \Omega(t)$, the set $x + \mathbf{B}(0, R)$ is known as the *sensing region* on which all the cells distributed at x, interact and form or break adhesion bonds with the cells located at $y \in \mathbf{B}(x, R) \cap \Omega(t)$. Further, $\mathbf{n}(y)$ denote the unit vector pointing from x to $x + y$, which is given by

$$\mathbf{n}(y) := \begin{cases} y/||y||_2 & \text{if} \quad y \in B(0, R) \setminus \{(0, 0)\}, \\ (0, 0) & \text{otherwise.} \end{cases} \tag{3}$$

The radially dependent spatial kernel $\mathcal{K}(\cdot)$ enable us to account for spatial distribution of the cells for both cell-cell and cell matrix adhesion within the sensing region $\mathbf{B}(x, R)$, and in the simulations we specifically use the form of $\mathcal{K}(\cdot)$ proposed in [16], namely

$$\mathcal{K}(r) := 1 - \frac{r}{R}, \tag{4}$$

where r is the radial distance between the centre point x and $y \in \mathbf{B}(x, R)$. This implies that for points in the sensing region $\mathbf{B}(x, R)$, as the distance r from x increases, the influence on adhesion-

driven migration decreases. The adhesion function $\mathbf{g}(t, \mathbf{u}(t, x+y))$ describes the local cell-cell and cell matrix adhesion. This explores the adhesion velocity of the cells at x is in the direction at which the cells can form the most bonds both among themselves and with components of the ECM within the sensing region around x. Here, $g_i(t, \mathbf{u}(t, x+y))$, $i = 1, 2$ denotes the $i-$th component of

$$\mathbf{g}(t, \mathbf{u}) = [\mathbf{S}_{cc}\mathbf{c} + \mathbf{S}_{cv}v] \cdot (1 - \rho(\mathbf{u}))^+, \tag{5}$$

and represents the cell-cell and cell matrix adhesion properties for population i, which are explicitly enable via the associated cell-cell and cell-matrix adhesion matrices, $\mathbf{S}_{cc}$, $\mathbf{S}_{cv} \in \mathbb{R}^{2,2}$, given by

$$\mathbf{S}_{cc} = \begin{bmatrix} S_{c_1,c_1} & S_{c_1,c_2} \\ S_{c_2,c_1} & S_{c_2,c_2} \end{bmatrix} \quad \text{and} \quad \mathbf{S}_{cv} = \begin{bmatrix} S_{c_1,v} & 0 \\ 0 & S_{c_2,v} \end{bmatrix}.$$

Furthermore, the overcrowding of the cell population and ECM is avoided through the term $(1-\rho(\mathbf{u}))^+ := \max\{(1-\rho(\mathbf{u})), 0\}$, which ensures that if a point in the domain is already overcrowded (with cells and/or ECM), then that space point does not contribute towards biasing the tumour cells migration due to adhesion.

As a tumour becomes increasingly malignant, it can obtain the ability to mutate to a more aggressive form of cancer cell. For this reason, $M_1(t, \mathbf{u})$ represents the mutation rate from population 1 to population 2. This mutation term is modelled as in [1, 15], namely

$$M_1(t, \mathbf{u}) = \delta H(t - t_{1,2}) \cdot H(v(t, x) - v_{\min}).$$

where $H(\cdot)$ denotes the usual Heaviside function and explore the fact that mutations from the primary tumour occur at a rate $\delta > 0$ after a certain time $t_{1,2}$ and in the presence of a minimal level v_{min} of ECM.

Within the tissue level, we must account the activity of the surrounding environment of the tumour; the extra-cellular matrix. Per unit time, the ECM exhibits degradation in the presence of cancer cells, along with a general remodelling of itself. Thus, this dynamics can be described mathematically as

$$\frac{\partial v}{\partial t} = -\gamma \mathbf{c} + \omega(1 - \rho(\mathbf{u})), \tag{6}$$

where: γ is the degradation coefficient multiplied by the current cancer cell distributions, and ω is the remodelling constant, here the matrix remodelling is controlled by the volume filling factor $(1-\rho(\mathbf{u}))$. Biological evidence suggests that the remodelling of the ECM is not only an essential role of development and wound healing, but also in the development of cancer, contributing to processes such as metastasis and tumour cell invasion [14].

2.2 Top-down tissue- to cell-scale link and the resulting microscopic dynamics.

As discussed previously, cancer cell invasion is a multiscale process in which the micro-dynamics of the matrix-degrading enzymes (MDEs) are responsible for the degradation of the ECM. The macroscopic processes defined by the equations (1) and (6) give rise to a micro-scale dynamics occurring along the invasive edge of the tumour, which, in turn, causes the macroscale boundary of the tumour to advance further into the healthy tissue, as schematically illustrated in Figure 2.

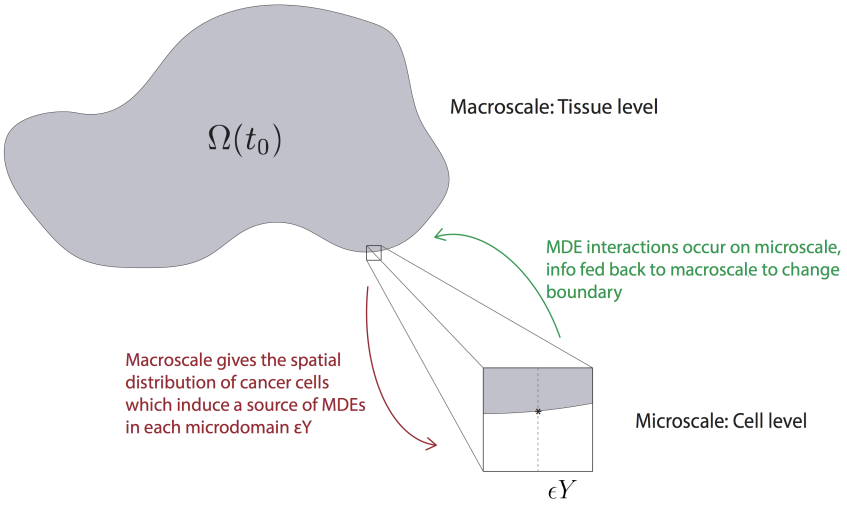

Fig. 2: *Schematic of macro-micro interactions.*

The MDEs, such as matrix metalloproteinasses (MMPs) of type 2, are produced within the cancer cells and distributed on the outer proliferating rim of the tumour, with their activity occurring

within the area directly surrounding the tumour. Specifically, during a time interval $[t_0, t_0 + \Delta t]$, the cancer cells arriving within the outer proliferating rim of the tumour secrete these MDEs giving rise to a source of such proteolytic enzymes that then exercise a cross-interface transport process within a cell-scale (microscale) size neighbourhood of $\partial\Omega(t_0)$, this way getting to interact directly and as a consequence significantly alter the ECM density that it meets in the peritumoural region. Hence, proceeding as described in [30], we denote by $\epsilon > 0$ the size of the micro-scale and we explore this MDEs micro-dynamics on an appropriate $\epsilon-$size neighbourhood of $\partial\Omega(t_0)$ given as the complete cover enabled by a union of half-way overlapping micro-cubes ϵY centred at the tumour interface. Thus, while assuming that we have no source for the cell-scale dynamics being formed outside $\Omega(t_0)$, at each instance $\tau \in [0, \Delta t]$ of the microdynamics and at each given micro-scale point $y \in \epsilon Y \cap \Omega(t_0)$ the source of MDEs is arising as a collective contribution of the cells from the outer proliferating rim that is located within a given distance $\delta > 0$ with respect to y. Therefore, denoting the source by $f_{\epsilon Y}(y, \tau)$, this is mathematically formulated as

$$
\begin{aligned}
&1. \quad f_{\epsilon Y}(y,\tau) = \frac{1}{\lambda(\mathbf{B}(y,\delta) \cap \Omega(t_0))} \int_{\mathbf{B}(y,\delta)\cap\Omega(t_0)} \alpha_1 c_1(x, t_0+\tau) + \alpha_2 c_2(x, t_0+\tau) dx, \quad y \in \epsilon Y \cap \Omega(t_0), \\
&2. \quad f_{\epsilon Y}(y,\tau) = 0, \quad y \in \epsilon Y \setminus \big(\Omega(t_0) + \{z \in Y |\ ||z||_2 < \gamma\}\big),
\end{aligned}
\tag{7}
$$

where $\lambda(\cdot)$ is the standard Lebesgue measure on $\mathbb{R}^2$, $\mathbf{B}(y,\delta) := \{x \in Y |\ ||y-x||_\infty \leq \delta\}$, α_i, $i = 1, 2$ are MDEs secretion rates by each of the two cell sub-populations, and γ is a small parameter enabling us to capture a sharp but smooth decay to 0 of the MDEs source immediately outside the tumour boundary.

Finally, as the $\epsilon-$size neighbourhood of $\partial\Omega(t_0)$ given by the bundle of half-way overlapping micro-cubes ϵY enables a decoupling of the micro-dynamics on individual ϵYs, in the presence of the source (7), we assume in this work that the MDEs are simply locally diffusing. Hence, denoting the density for MDEs by $m(y, \tau)$, in each ϵY the micro-dynamics exercised by the MDEs is described by:

$$
\frac{\partial m}{\partial \tau} = \Delta m + f_{\epsilon Y}(y,\tau), \qquad y \in \epsilon Y,\ \tau \in [0, \Delta t]. \tag{8}
$$

Macroscopic boundary movement induced by microscale. During their micro-dynamics, the MDEs interact with the ECM components in the peritumoural region captured by each ϵY. As described in [30], according to the spatial distribution of their advancing front on $\epsilon Y \setminus \Omega(t_0)$, the MDE cause specific spatial patterns of degradation of the ECM components that determine completely a direction of movement $\eta_{_{\epsilon Y}}$ and displacement magnitude $\xi_{_{\epsilon Y}}$ for the tumour boundary progression within each ϵY. As illustrated schematically in Figure 3, this choreographic movement of the tumour boundary captured by the micro-domain ϵY is represented back at macro-scale through the relocation of the tumour boundary midpoint $x^*_{\epsilon Y}$, which is located at the intersection of $\partial\Omega(t_0) \cap \epsilon Y$ with the median of ϵY perpendicular to the side of ϵY inside the cancer region, this being chosen as the inner most point in this intersection with respect to the cancer region. Thus, following the derivation in [30], using an appropriately chosen dyadic decomposition of ϵY in a union of small dyadic cubes $\{D_l\}_{i=1,p_{_{\epsilon Y}}}$, with $p_{_{\epsilon Y}} := 2^{k_{\epsilon Y}}$, that ensure uniformity of the approach across all the boundary micro-domains ϵY, the direction of movement $\eta_{_{\epsilon Y}}$ and displacement magnitude $\xi_{_{\epsilon Y}}$ for the point $x^*_{\epsilon Y}$ are determined mathematically, and are given by

$$\eta_{\epsilon Y} = x^*_{\epsilon Y} + \nu \sum_{l \in \mathcal{I}^*_{\epsilon Y}} \left(\int_{\mathcal{D}_l} m(y, \tau_f)\ dy \right) (y^*_l - x^*_{\epsilon Y}),$$

$$\xi_{\epsilon Y} = \sum_{l \in \mathcal{I}^*_{\epsilon Y}} \frac{\int_{\mathcal{D}_l} m(y, \tau_f)\ dy}{\sum\limits_{l \in \mathcal{I}^*_{\epsilon Y}} \int_{\mathcal{D}_l} m(y, \tau_f)\ dy} |\overrightarrow{x^*_{\epsilon Y} y_l}|.$$

where, $\mathcal{I}^*_{\epsilon Y}$ are the family of indices of the dyadic cubes that track the tip of the advancing MDEs front in ϵY, and y_l represents the baricenter of D_l for any $l \in \mathcal{I}^*_{\epsilon Y}$.

Although a movement direction and displacement have been derived for each $x^*_{\epsilon Y}$, movement will only occur if the ECM degradation is of a certain local strength. The strength of this local ECM degradation is explored through the transitional probability q^* defined in [30] and it is a quantification of the amount of MDE in $\epsilon Y \setminus \Omega(t_0)$ relative to the total amount of MDE in the micro domain ϵY. Therefore the midpoint $x^*_{\epsilon Y}$ will only move to a new spatial position if and only if $q^*(x^*_{\epsilon Y}) := q^*(\epsilon Y \setminus \Omega(t_0))$ exceeds a certain threshold $\omega_{\epsilon Y} \in (0, 1)$ that captures local peritumoural tissue characteristics. Hence, we find that the new invasive boundary $\partial\Omega(t_0 + \Delta t)$ will be an interpolation of the new locations for the points that exercised the movement and those boundary points $x^*_{\epsilon Y}$ that did not move. The invasion process will continue on the newly expanded domain $\Omega(t_0 + \Delta t)$ with a new set of macro-micro stage dynamics on the next multiscale time step

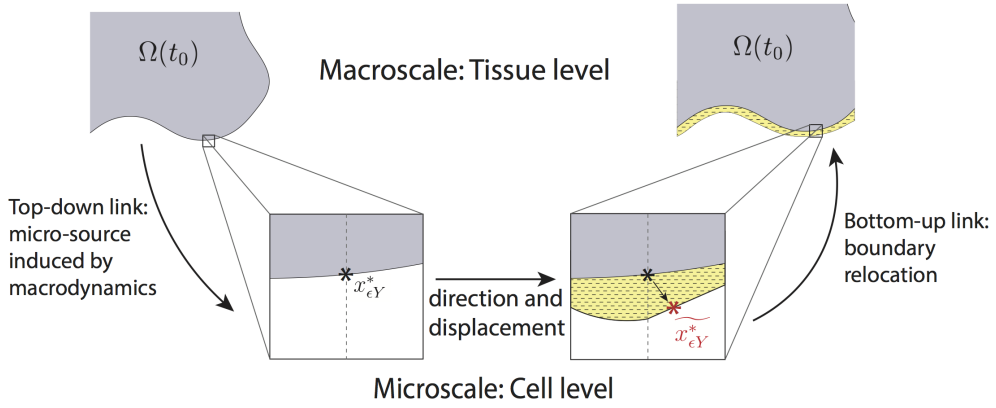

Fig. 3: *Schematic of one macro-micro stage in the multiscale process. The projected ϵY cube from macro- to micro-scale with boundary point reallocation occuring through the micro dynamics and the new relocated boundary position projected back into the macroscopic scale at the tissue level.*

$[t_0 + \Delta t, t_0 + 2\Delta t]$. The initial conditions on the expanded domain $\Omega(t_0 + \Delta t)$ are determined by the solution at the final time of the previous invasion step, as detailed in [30].

2.3 Summary of the Global Multiscale Model

At each stage of the invasion process, the macroscale dynamics govern the spatial distributions of both cancer cell populations and the ECM density. The initial distribution of cancer cells $\Omega(t_0)$ induce a source of MDEs (7) on the boundary at each microdomain ϵY. The microscopic dynamics induce a change in the boundary position as illustrated in Figure 3. This movement is then translated back into the macroscale, where the new spatial positions of the boundary $\widetilde{x^*_{\epsilon Y}}$ are interpolated with the spatial positions that could not be moved and a new invading edge in obtained as illustrated in Figures 2 and 3. The next macro-micro stage will then proceed using the solution from the previous step as the new initial conditions and invasion will continue. Once the invasion process has advanced, mutations will begin to occur between cell populations. The mutated population c_2 carries a higher malignancy than population c_1, thus it secretes a higher volume of MDEs, which in turn will allow the second population to advance quicker.

3 Numerical approaches and simulations

The numerical scheme developed for the multiscale model described above is structured on two big components corresponding to the macro- and micro- scales processes involved, namely: (1) a finite differences based macro-solver that addresses the macro-dynamics; and (2) a finite element micro-slover exploring the micro-dynamics that is based on a standard approach involving bilinear shape functions on a squared mesh for each micro-domain. As the macro-solver involves a special treatment for the adhesion terms $\mathcal{A}_n$, in the following we will highlight the main features that this involves.

3.1 Brief description of scheme developed for the macro-scale solver

As already mentioned above, an important aspect within the macroscopic part of our solver is the numerical approach for the adhesive fluxes $\mathcal{A}_n$ (that explores the effects of cell-cell and cell-matrix adhesion of population c_n), which involves off-grid computations and we address these as follows. We decompose the sensing region $\mathbf{B}(x,R)$ in $s2^m$ annulus radial sectors $\mathcal{S}_1,\ldots,\mathcal{S}_{2^m}$ (obtained by intersecting s annuli with 2^m uniform radial sectors of $\mathbf{B}(x,R)$, as shown in Figure 4, with the radius of the central circle taken small enough so that this is neglected in the subsequent computation steps). Then, for each S_l, we evaluate the total population c_1, total population c_2, and the total ECM mass distributed on $\mathcal{S}_l$ that are given by

$$\omega_{\mathcal{S}_l,c_1}(t) := \frac{1}{\lambda(\mathcal{S}_l)}\int\limits_{\mathcal{S}_l} c_1(t,x)dx, \quad \omega_{\mathcal{S}_l,c_2}(t) := \frac{1}{\lambda(\mathcal{S}_l)}\int\limits_{\mathcal{S}_l} c_2(t,x)dx, \quad \textit{and} \quad \omega_{\mathcal{S}_l,v}(t) := \frac{1}{\lambda(\mathcal{S}_l)}\int\limits_{\mathcal{S}_l} v(t,x)dx,$$

respectively. Finally, denoting by $\mathbf{b}_{\mathcal{S}_l}$ the barycenter of $\mathcal{S}_l$, $\forall l = 1,\ldots,s2^m$ and evaluating the unit vector $\mathbf{n}(\mathbf{b}_{\mathcal{S}_l}) := \frac{\mathbf{b}_{\mathcal{S}_l}-x}{\|\mathbf{b}_{\mathcal{S}_l}-x\|_2}$, the adhesion flux $\mathcal{A}_n$, $n=1,2$, is approximated by

$$\mathcal{A}_n(t,x,\mathbf{u}(t,\cdot)) = \sum_{\substack{l=1 \\ \mathbf{b}_{\mathcal{S}_l}\cap\Omega(t_0)\neq\emptyset}}^{s2^m} \frac{\lambda(\mathcal{S}_l)}{R}\mathbf{n}(\mathbf{b}_{\mathcal{S}_l})\cdot\mathcal{K}(\mathbf{b}_{\mathcal{S}_l})g_n(\tilde{\mathbf{u}}(t,\mathbf{b}_{\mathcal{S}_l}))$$

where

$$\tilde{\mathbf{u}}(t, \mathbf{b}_{\mathcal{S}_l}) := [\omega_{\mathcal{S}_l,c_1}(t), \omega_{\mathcal{S}_l,c_2}(t), \omega_{\mathcal{S}_l,v}(t)]^T$$

and

$$g_n(\tilde{\mathbf{u}}(t, \mathbf{b}_{\mathcal{S}_l})) = [\mathbf{S}_{cc}[\omega_{\mathcal{S}_l,c_1}(t), \omega_{\mathcal{S}_l,c_2}(t)]^T + \mathbf{S}_{cv}\omega_{\mathcal{S}_l,v}(t)] \cdot (1 - \rho(\tilde{\mathbf{u}}(t, \mathbf{b}_{\mathcal{S}_l})))^+$$

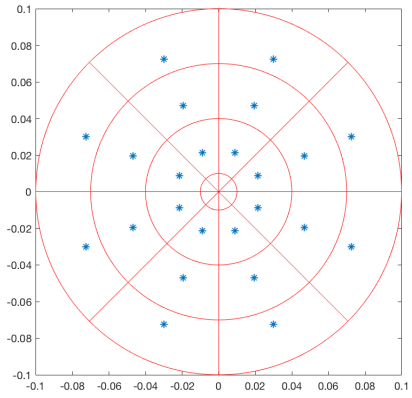

Fig. 4: *Sensing region* $\mathbf{B}(x, R)$ *approximated by the annulus radial sectors with the barycentre* $\mathbf{b}_{\mathcal{S}_l}$ *associated to each sector* $\mathcal{S}_l$ *highlighted with a blue dot.*

For the actual implementation, we discretise the entire domain Y by considering a uniform spatial mesh of size h, i.e., $\Delta x = \Delta y = h$ as well as the time interval $[t_0, t_0 + \Delta t]$ into k uniformly distributed time steps, i.e., $\delta_\tau = \frac{\Delta t}{k}$. In order to approximate the reaction-diffusion equations (1), we develop a predictor-corrector in time scheme; whilst the term $\nabla \cdot [\nabla c_n - c_n \mathcal{A}_n(t, x, \mathbf{u}(t, \cdot))]$ will be approximated by a second-order mid-point rule.

In brief, for any time step of index $p = 0, ..., k$ and for the spatial nodes (i, j), where $i = 1, ..., q$, $j = 1, ..., q$ are the indices for the $x-$ and y-direction, respectively, we introduce the midpoint approximations as:

$$\begin{cases} c^p_{n,i,j+\frac{1}{2}} := \frac{c^p_{n,i,j} + c^p_{n,i,j+1}}{2} \\ c^p_{n,i,j-\frac{1}{2}} := \frac{c^p_{n,i,j} + c^p_{n,i,j-1}}{2} \\ c^p_{n,i+\frac{1}{2},j} := \frac{c^p_{n,i,j} + c^p_{n,i+1,j}}{2} \\ c^p_{n,i-\frac{1}{2},j} := \frac{c^p_{n,i,j} + c^p_{n,i-1,j}}{2} \end{cases} \quad \text{and} \quad \begin{cases} \mathcal{A}^p_{n,i,j+\frac{1}{2}} := \frac{\mathcal{A}^p_{n,i,j} + \mathcal{A}^p_{n,i,j+1}}{2} \\ \mathcal{A}^p_{n,i,j-\frac{1}{2}} := \frac{\mathcal{A}^p_{n,i,j} + \mathcal{A}^p_{n,i,j-1}}{2} \\ \mathcal{A}^p_{n,i+\frac{1}{2},j} := \frac{\mathcal{A}^p_{n,i,j} + \mathcal{A}^p_{n,i+1,j}}{2} \\ \mathcal{A}^p_{n,i-\frac{1}{2},j} := \frac{\mathcal{A}^p_{n,i,j} + \mathcal{A}^p_{n,i-1,j}}{2} \end{cases}$$

We also have the following notation for the central differences:

$$\begin{cases} [c_{n,y}]^p_{i,j+\frac{1}{2}} := \frac{c^p_{n,i,j}-c^p_{n,i,j+1}}{\Delta y} \\ [c_{n,y}]^p_{i,j-\frac{1}{2}} := \frac{c^p_{n,i,j}-c^p_{n,i,j-1}}{\Delta y} \\ [c_{n,x}]^p_{i+\frac{1}{2},j} := \frac{c^p_{n,i,j}-c^p_{n,i+1,j}}{\Delta x} \\ [c_{n,x}]^p_{i-\frac{1}{2},j} := \frac{c^p_{n,i,j}-c^p_{n,i-1,j}}{\Delta x} \end{cases}$$

Using this notation, the approximation for (ignoring the constant parameters at the moment) $\nabla \cdot [\nabla c_n - c_n \mathcal{A}_n(t,x,\mathbf{u}(t,\cdot))]$ in (1) is as follows:

$$\begin{aligned} \nabla \cdot [\nabla c_n - c_n \mathcal{A}_n(t,x,\mathbf{u}(t,\cdot))] &= \mathrm{div}[\nabla c_n - c_n \mathcal{A}_n(t,x,\mathbf{u}(t,\cdot))]^p_{i,j} \\ &\simeq \frac{[c_{n,x}]^p_{i+\frac{1}{2},j} - [c_{n,x}]^p_{i-\frac{1}{2},j} - c^p_{n,i+\frac{1}{2},j} \cdot \mathcal{A}^p_{n,i+\frac{1}{2},j} + c^p_{n,i-\frac{1}{2},j} \cdot \mathcal{A}^p_{n,i-\frac{1}{2},j}}{\Delta x} \\ &+ \frac{[c_{n,y}]^p_{i,j+\frac{1}{2}} - [c_{n,y}]^p_{i,j-\frac{1}{2}} - c^p_{n,i,j+\frac{1}{2}} \cdot \mathcal{A}^p_{n,i,j+\frac{1}{2}} + c^p_{n,i,j-\frac{1}{2}} \cdot \mathcal{A}^p_{n,i,j-\frac{1}{2}}}{\Delta y} \end{aligned} \tag{9}$$

For the time discretisation of equation (6), following [30], we have used a predictor-corrector method, where the predictor is given by a second-order Adams-Bashforth scheme and the corrector uses a second-order trapezoidal approximation.

3.2 Simulations in two spatial dimensions

To explore numerically multiscale model of cancer invasion given in (1)-(8), we consider region $Y := [0,4] \times [0,4]$ discretised uniformly with macroscopic spatial step size $h = 0.03125$, while the time step is taken here as $\delta_\tau = 10^{-3}$. Assuming that initially population c_2 has no distribution and population c_1 occupies a region $\Omega(0) := \mathbf{B}((2,2),0.5)$ positioned at the centre of the domain Y. The initial condition for cancer cell population c_1 is taken as in [30] and is given by

$$c_1(0,x) = 0.5\left(\exp\left(-\frac{||x-(2,2)||_2^2}{0.03}\right) - \exp(-28.125)\right)\left(\chi_{\mathbf{B}((2,2),0.5-\gamma)} * \psi_\gamma\right),$$

where ψ_γ is the mollifier defined in [30] with $\gamma << \frac{\Delta x}{3}$. Population c_2 initially has zero density, so $c_2(0,x) = 0$ and we assume a heterogeneous distribution for the initial ECM density based on the initial condition proposed in [15] and given by

$$v(0,x) = \min\left\{h(x_1,x_2), \frac{1-\vartheta_c c(0,x)}{\vartheta_v}\right\}, \tag{10}$$

where

$$h(x_1,x_2) = \frac{1}{2} + \frac{1}{2}\sin(\zeta x_1 x_2)^3 \cdot \sin(\zeta\frac{x_2}{x_1}), \tag{11}$$

with

$$(x_1,x_2) = \frac{1}{3}(x+1.5) \ \in [0,1]^2 \text{ for } x \in D, \quad \zeta = 7\pi.$$

Here we consider the volume fraction of cells and ECM to be $\vartheta_c \in [\frac{\pi}{6}, 1]$ and $\vartheta_v \in [0, \frac{5\pi}{6}]$. The initial condition for MDEs is $m(0,x) = 0.5c_1(0,x)$, however since this closely resembles the profile of the cancer cell distribution, we shall not present the simulation results of MDE concentration. The initial conditions of the combined cell populations and ECM density can be seen in Figure 5.

Throughout these simulations, unless otherwise stated, we use the following parameter set for the non-dimensionalised system of equations (1) and (6), which were estimated based on those used in [15], namely:

$$\mathcal{P}: \quad \begin{aligned} &D_1 = 10^{-3},\, D_2 = 10^{-3}, \ \ \gamma = 2, \quad t_{1,2} = 10, \ \ \delta = 0.3, \\ &\mu_1 = 0.25, \quad \mu_2 = 0.25, \quad \omega = 0, \ \ v_{\min} = 0.3 \end{aligned}$$

We also have here the adhesive strengths matrices $\mathbf{S}_{cc}$ and $\mathbf{S}_{cv}$ given by

$$\mathbf{S}_{cc} = \begin{pmatrix} 0.5 & 0 \\ 0 & 0.3 \end{pmatrix} \quad \text{and} \quad \mathbf{S}_{cv} = \begin{pmatrix} 0.3 & 0 \\ 0 & 0.6 \end{pmatrix}. \tag{12}$$

Initially, we have no cross-adhesion occurring, so $S_{c_1,c_2} = 0 = S_{c_2,c_1}$.

Figure 7 gives simulations using the initial conditions and parameter set $\mathcal{P}$ as stated above. They are shown at stages $25\Delta t,\ 50\Delta t$ and $75\Delta t$. Here, we also show the simulations at stage $10\Delta t$, Figure 6, the stage at which mutations occur. By this stage, population c_1 has degraded and lowered the density of the ECM in which the initial cancer distribution was placed. The threshold on which mutations can occur, δ, is higher than the resulting density of ECM, thus when mutations occur, they only take place on the outer edge of the tumour, where $\delta > 0$, as the ECM density is too low inside to support the mutations. The white contour shows the proliferating boundary of the tumour,

(a) initial ECM density (b) initial cancer distribution

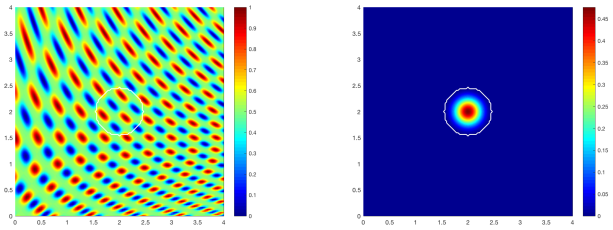

Fig. 5: *Initial conditions of the density of ECM (a) and the distribution of cancer cells (b) with the invasive boundary of the tumour represented by the white contour.*

(a) population c_1 (b) population c_2

(c) combined cell populations (d) ECM density

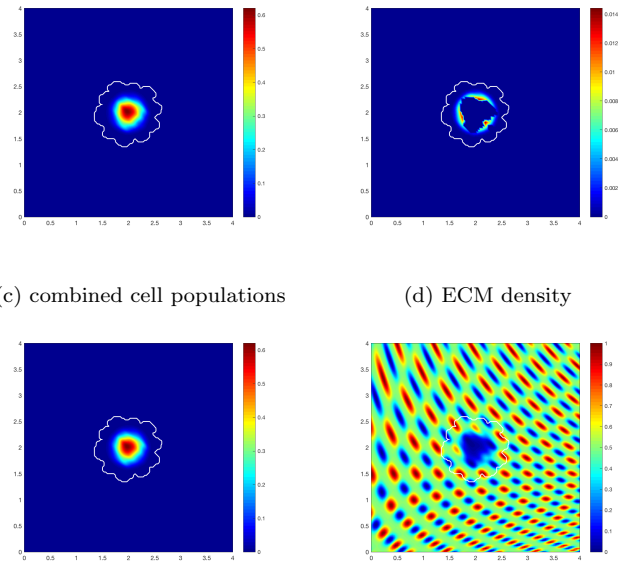

Fig. 6: *Simulation results of model at stage* $10\Delta t$ *when the mutations from population* c_1 *start to occur.*

which, at this stage has consistently expanded outwards into the ECM. Due to the initial conditions of the ECM, there are patches of high and low density areas throughout the domain. These patches vary in distance and size from one another, which reflects a non-symmetric microenvironment for

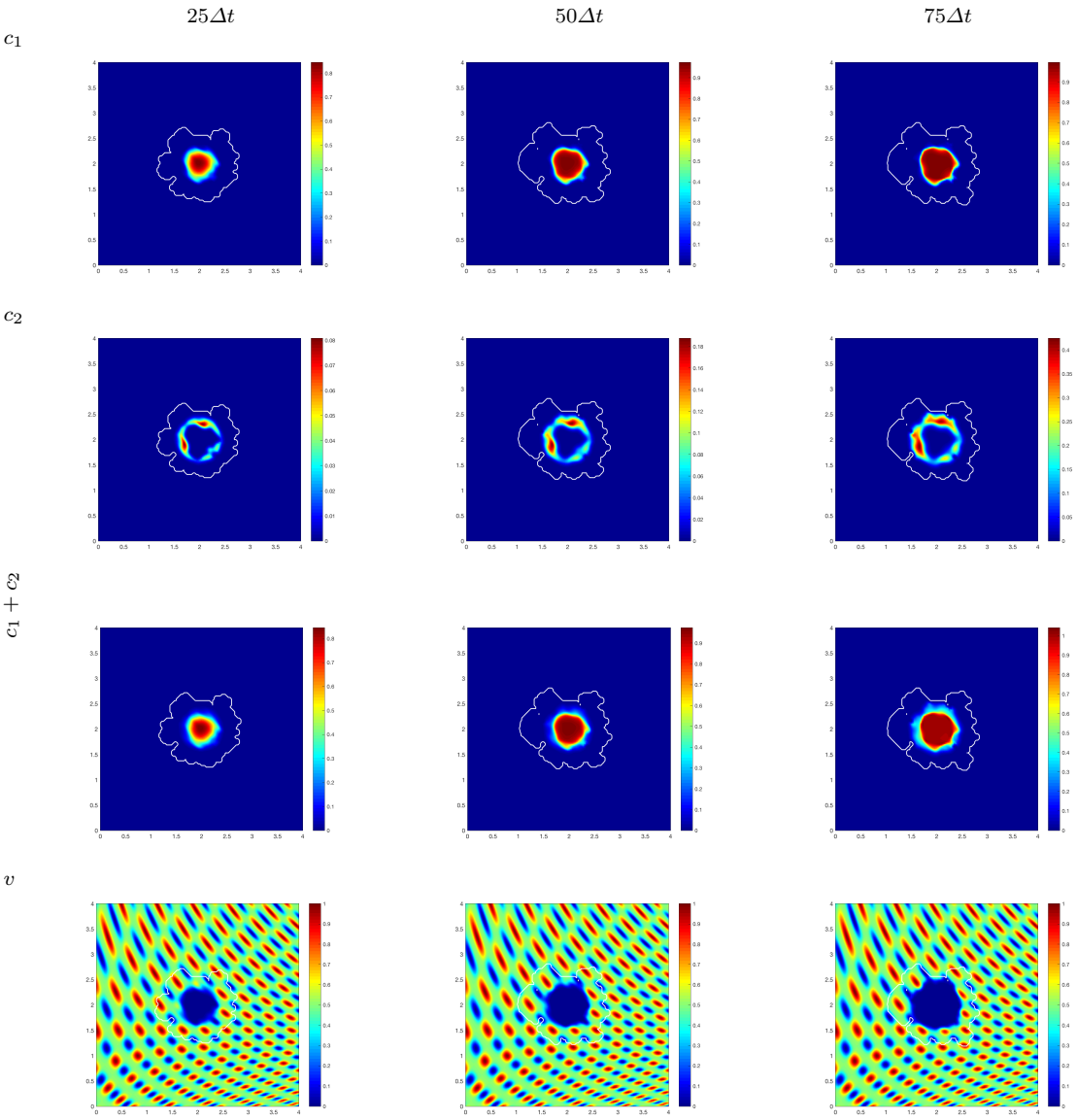

Fig. 7: *Simulation results of model using the parameter set* $\mathcal{P}$ *and adhesion matrices (12). Plots of both cancer populations* c_1 *and* c_2*, as well as the combined cancer distributions and the ECM densities at stages* $25\Delta t$*,* $50\Delta t$*, and* $75\Delta t$*.*

the cells. The pattern of the advancing front of the tumour loosely follows this pattern of ECM. Where there are dense patches of low density we see slower cancer progression; this is because there is a lower overall density of matrix for the cells to adhere.

After 25 macro-micro stages, $25\Delta t$, population c_1 and c_2 are both increasing in density, with population c_1 changing shape as the cells continue to mutate. As the tumour spreads, a larger region of ECM is degraded, which is shown in the plot for ECM.

As the cancer continues to invade, a wider region of the ECM is destroyed and the proliferating edge of the tumour continues to reach outwards, see stages $50\Delta t$ and $75\Delta t$ in Figure 7. The invasive edge of the tumour loosely follows the pattern of ECM at each stage, and small islands start to appear over low density patches of ECM. These islands have zero ECM density and hence cause the cancer cells to be slow to invade as there is an insufficient level of ECM for which the cells can adhere. This pattern of the boundary is due to the multiscale nature of the invasion process, where the macro-dynamics govern the source of the MDEs on the invading edge and then movement of the boundary is determined in each boundary cube ϵY by the resulting micro-dynamics. The MDEs produced by the cancer cells can only degrade locally; this becoming apparent from the resulting ECM plots.

We now want to consider the effect of matrix remodelling on the progression of cancer. Figure 8 shows simulations again using the parameter set $\mathcal{P}$, but this time with the ECM remodelling rate ω being increased from 0 to 0.04. Here we see that the spread of cancer is ultimately covering a larger area than in the absence of remodelling, Figure 7. Population c_2 displays a much larger spread of density surrounding population c_1 than in the absence of ECM remodelling. The increased density of ECM surrounding the cells gives more opportunity for adherence and opens a greater number of pathways in which the cells can invade. The boundary of the cancer is following the pattern of the ECM more consistently than in Figure 7, this is due to the higher density of the remodelled ECM allowing for stronger adhesive qualities between the cancer cells and ECM. We can again see the invasion briefly halted at patches of lower density, but this is for a shorter period than before, with the islands being fully invaded by the later stages.

Figure 9 gives simulations where the cell-matrix adhesion between cancer cell population c_1 and the ECM, $S_{c_1,v}$, has been increased from 0.3 to 0.5 and the cell-matrix adhesion between cell population c_2 and the ECM, $S_{c_2,v}$, has been decreased from 0.6 to 0.5, i.e., the adhesion rate between the cells and matrix are equal for both populations. The proliferating edge of the tumour

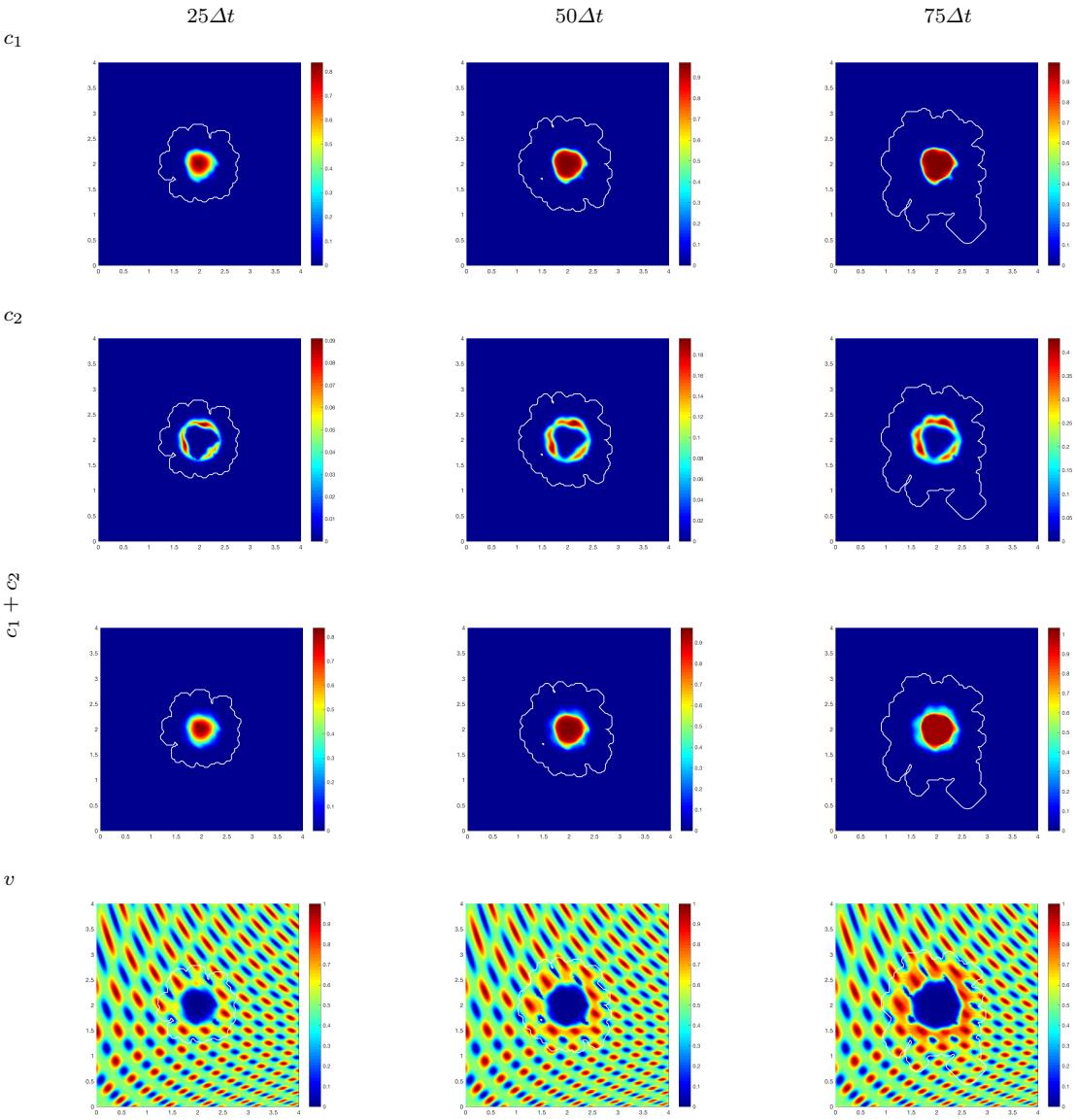

Fig. 8: *Simulation results of model with ECM remodelling introduced,* $\omega = 0.04$*, with the same parameter set* $\mathcal{P}$ *and adhesion matrices as in Figure 7.*

is lobular in the way it follows the pattern of the ECM, much like the simulations in Figure 7, with protrusions pushing out in the direction of high density areas of the matrix. Although the cell-matrix adhesion term is now equal for both populations, the S_{c_1,c_1} and S_{c_2,c_2} have remained the same, thus we do not see a great change in the profile of the levels of cancer cell densities of the main body of the tumour itself, but we instead see a difference in the pattern of the invading edge of the tumour, due to the further spread of the lower levels of these densities closer to the invasive edge of the tumour. The increase in adhesion between population c_1 and the matrix sees the invading boundary stick closer to the main body of the tumour, particularly to population c_2.

Finally, we investigate the effects of cell-cell adhesion and in particular cross-adhesion. Cross-adhesion is when different cancer cell populations adhere to one another. Here we set $S_{c_1,c_2} = S_{c_2,c_1}$ as both populations will have the same rate of adherence to each other. We look at the case using parameter set $\mathcal{P}$ and the adhesion matrices

$$\mathbf{S}_{cc} = \begin{pmatrix} 0.5 & 0.5 \\ 0.5 & 0.3 \end{pmatrix} \quad \text{and} \quad \mathbf{S}_{cv} = \begin{pmatrix} 0.3 & 0 \\ 0 & 0.6 \end{pmatrix}, \tag{13}$$

Our simulations in this case, shown in Figure 10, exhibit the same general morphology of the tumour boundary as in results with no cross-adhesion present, mainly due to the fact that in this work both cancer cell population are assumed to degrade the ECM at the same rate. However, the difference with respect to the no cross-adhesion case is emphasized by the spatial distribution of the two cancer cell populations within the main body of the tumour. Population c_1 remains consistent with results computed in Figure 7, however population c_2 exhibits different behaviour. We can distinguish now two higher density patches of c_2 densities which do not spread away from the significantly high levels of c_1 cell density and rather build up in their immediate proximity. Combining the cell populations now gives an increasingly contained spread of the tumour. This result is to be expected because the cells are now more inclined to stick together, rather than invade outwards, and although the adherence between cell populations has increased, their adhesion towards the matrix has stayed the same, hence we observe no difference in the movement of the boundary. This difference is also consistent with the other no cross-adhesion cases considered in Figs. 8 and 9.

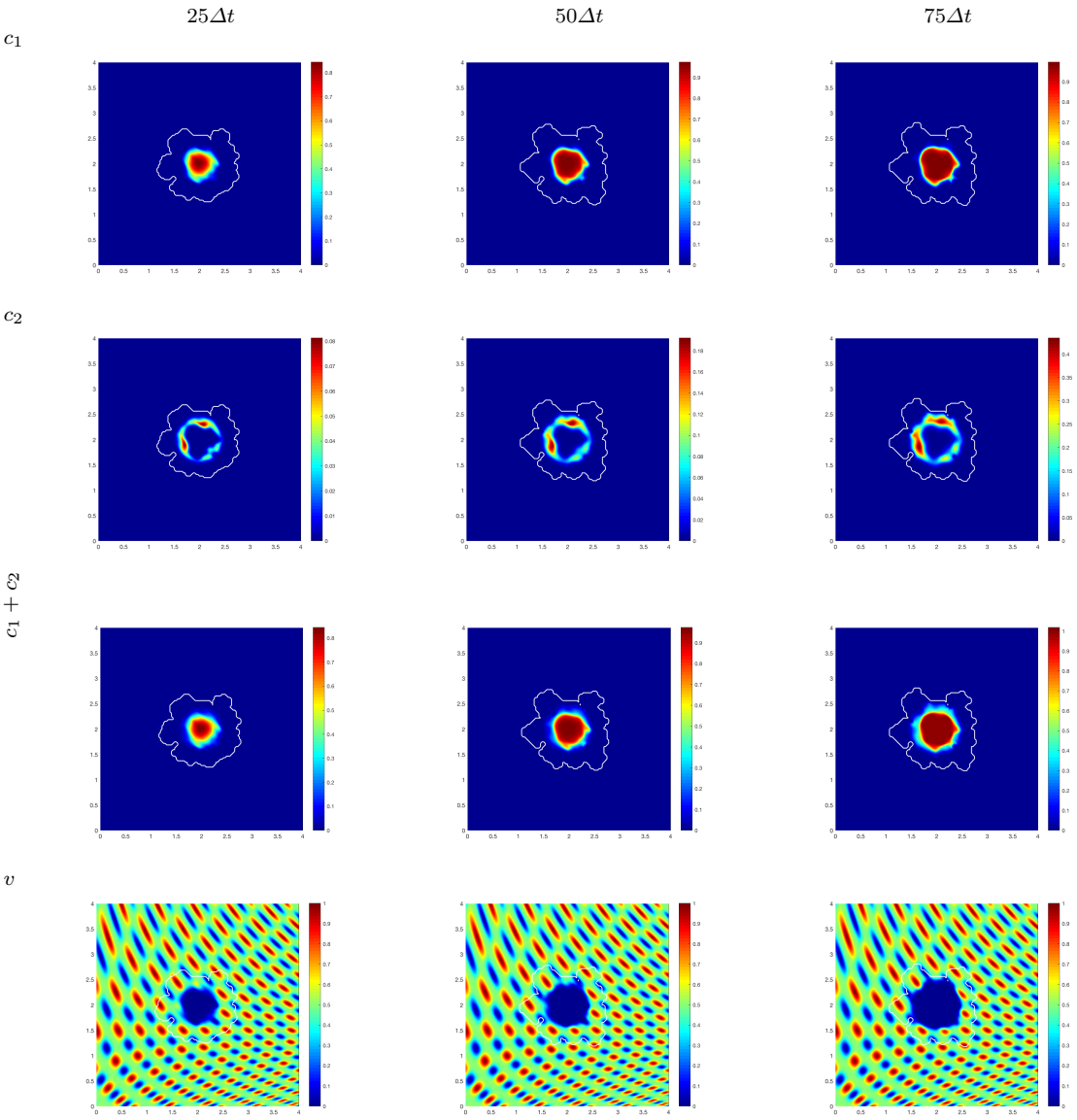

Fig. 9: *Simulation results of model with parameter set* $\mathcal{P}$ *and* $S_{c_1,v} = 0.5 = S_{c_2,v}$.

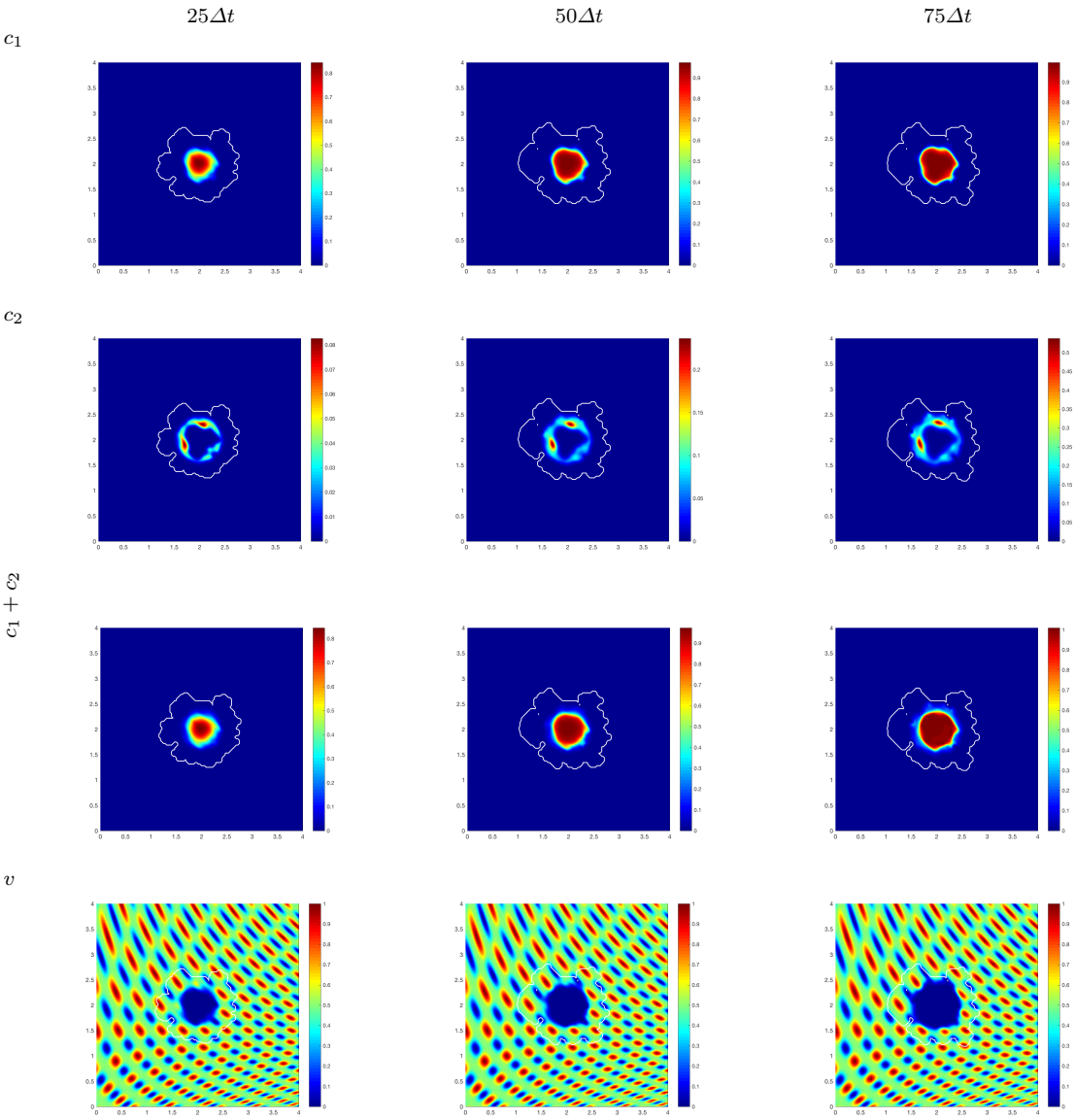

Fig. 10: *Simulation results of model with parameter set $\mathcal{P}$ with cross-adhesion coefficient* $S_{c_1,c_2} = 0.5 = S_{c_2,c_1}$.

3.3 Sensitivity to Initial Conditions

To address sensitivity with respect to initial data, we present and discuss here the results of four different sets of initial conditions for the ECM that are induced (10) with (11) by function h given in (14), which are gradually convergent towards the case of homogeneous ECM. Figure 11(a) illustrates a homogenous ECM induced in (10) by the limit case for h that we obtain as $n \to \infty$, namely $h(x_1, x_2) = \frac{1}{2}$. Figure 11(b) and 11(c) use the initial condition (10), where the equation for $h(x_1, x_2)$ is changed to

$$h(x_1, x_2) = \frac{1}{2} + \frac{1}{2^n} \sin(\zeta x_1 x_2)^3 \cdot \sin(\zeta \frac{x_2}{x_1}), \tag{14}$$

with $n = 3, 5$ for Figure 11(b) and 11(c), respectively. Using this form effectively flattens down the high density regions of the heterogeneous ECM, making it progressively closer to a homogeneous case, who exhibits a symmetric growth. Finally, Figure 11(d) shows the simulations using the initial conditions (10) with (11), as in Figure 7. The main body of the tumour remains similar from each initial condition of ECM as all coefficients remain the same as in the no cross-adhesion case shown in Figure 7. The differences between the invading boundaries are clearly visible, ranging from a symmetric expansion of the boundary for homogeneous initial conditions to a fingering leading edge for heterogeneous conditions. We conclude that as the initial condition for the ECM becomes increasingly heterogeneous, the proliferating edge of the tumour becomes consistently more lobular in its invasion.

4 Conclusions

We have presented a multiscale moving boundary model which builds on previous framework proposed by [30] by exploring adhesive dynamics [15] between a heterogeneous cancer cell population and the surrounding microenvironment. This considers both the macro-scale dynamics of two cancer cell sub-populations within the ECM and their influence on the micro-scale MDEs molecular dynamics occurring at the cell-scale along the invasive edge of the tumour. This macro-micro top-down link is given here via the source of MDEs that are secreted by the cancer cells from both c_1 and c_2 sub-populations arriving within the outer proliferating rim of the tumour. In turn, the micro-

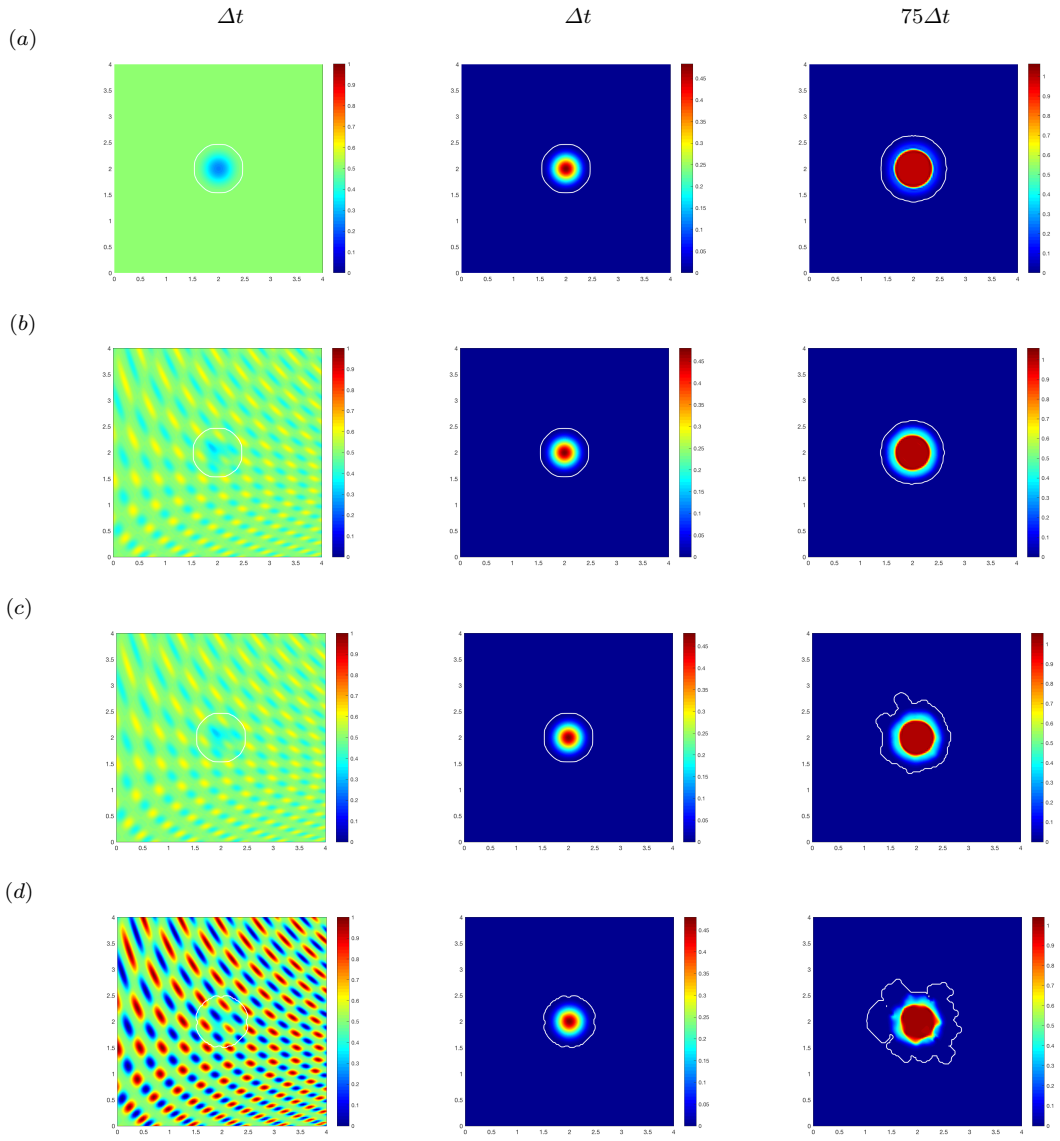

Fig. 11: *Simulation results showing different initial conditions for the ECM. Plots showing ECM and the combined cancer distribution at their initial stage* Δt*, and the tumour at final stage* $75\Delta t$*.*

dynamics occurring on the cell-scale enables a micro-macro feedback in the form of a bottom-up link by providing the movement direction and displacement magnitude of the tumour boundary.

Comparing with results from the previous framework proposed in [30], we have shown that the inclusion of cell-cell and cell-matrix adhesion changes the way in which the cancer progresses. The computational results presented in this chapter have shown that the initial tumour region exercises greater movement than in the absence of adhesive qualities. We then incorporate another cell population and further explore the interactions between both cancer cell populations and their microenvironment. We have shown that in the presence of ECM remodelling, there is a greater spread of cancer cells as there is more opportunity for adherence which allows the cells to move. Increased cell-matrix adhesion, in particular between c_1 and v, has shown that a change in cell-matrix adhesion will not necessarily change the main body of the tumour, but it induces a change in the invading boundary, becoming very lobular when following the pattern of the ECM. Adding cross-adhesion to these models has shown how the different cell populations mix with one another and exhibits a denser region of population c_2 which remain in the proximity of highest regions of c_1 density. Finally, we investigated the effects of varying initial conditions of ECM, starting with a homogeneous distribution and becoming increasingly heterogenous. We have concluded that as the initial ECM distribution increases in heterogeneity, the proliferating boundary of the tumour becomes more lobular.

To gain further understanding of how cancer cells invade, focus must be placed on the surrounding microenvironment. The extracellular matrix is made from many different components, most of which play a vital role in cancer invasion. The main component of the ECM is collagen, particularly collagen type I which provides the matrix with its structure and flexibility. Investigations into the mesenchymal motion of tumour cells [13, 19, 25], shows that the difference between *undirected* and *directed* fibres is of high importance. Undirected fibres are symmetrical along their axes and their direction is identical at both ends, an example of this type of fibre would be collagen in the human body. Unlike undirected fibres, directed fibres are unsymmetrical and can be distinguished at both ends. Recent work considering fibres by [31], focussed on directed fibres, have highlighted differences between directed and undirected fibres using a one-dimensional model. The addition of fibres, directed or undirected, into the multiscale model would greatly change the pattern of invasion. Several other components of the ECM such as fibronectin, laminin and a variety of different MMPs are also vital in tumour invasion and a greater mathematical understanding of these would allow for an overall better understanding of cancer progression.

Acknowledgment

RS and DT would like to acknowledge the support received through the EPSRC DTA Grant EP/M508019/1 on the project: *Multiscale modelling of cancer invasion: the role of matrix-degrading enzymes and cell-adhesion in tumour progression.*

References

[1] Andasari, V., Gerisch, A., Lolas, G., South, A., Chaplain, M.A.J., 2011. Mathematical modeling of cancer cell invasion of tissue: biological insight from mathematical analysis and computational simulation. *J. Math. Biol.* **63**(1), 141–171.

[2] Anderson, A., Rejniak, K., Gerlee, P., Quaranta, V., 2007. Modelling of cancer growth, evolution and invasion: Bridging scales and models. *Math Model Nat Phenom* **2**(3), 1–29.

[3] Anderson, A.R.A., Chaplain, M.A.J., Newman, E.L., Steele, R.J.C., Thompson, A.M., 2000. Mathematical modelling of tumour invasion and metastasis. *J Theor Med* **2**(2), 129–154. doi:10.1080/10273660008833042.

[4] Armstrong, N.J., Painter, K.J., Sherratt, J.A., 2006. A continuum approach to modelling cell-cell adhesion. *J. Theor. Biol.* **243**(1), 98–113.

[5] Bellomo, N., Angelis, E.D., Preziosi, L., 2002. Multiscale modelling and mathematical problems related to tumour evolution and medical therapy. *J Theor Biol* **58**, 3719–3727.

[6] Berrier, A.L., Yamada, K.M., 2007. Cell-matrix adhesion. *J Cell Physiol* **213**(3), 565–573. doi:10.1002/jcp.21237.

[7] Bhagavathula, N., Hanosh, A.W., Nerusu, K.C., Appelman, H., Chakrabarty, S., Varani, J., 2007. Regulation of e-cadherin and β-catenin by Ca^{2+} in colon carcinoma is dependent on calcium-sensing receptor expression and function. *Int J Cancer* **121**, 1455–1462. doi:10.1002/ijc.22858.

[8] Byrne, H.M., Preziosi, L., 2004. Modelling solid tumour growth using the theory of mixtures. *Math Med Biol* **20**, 341–366. doi:10.1093/imammb/20.4.341.

[9] Cavallaro, U., Christofori, G., 2001. Cell adhesion in tumor invasion and metastasis: loss of the glue is not enough. *Biochimica et Biophysica Acta (BBA) - Reviews on Cancer* **1552**(1),

39–45. doi:10.1016/S0304-419X(01)00038-5.

[10] Chaffer, C.L., Weinberg, R.A., 2011. A perspective on cancer cell matastasis. *Science* **331**(6024), 1559–1564.

[11] Chaplain, M.A., 1996. Avascular growth, angiogenesis and vascular growth in solid tumours: The mathematical modelling of the stages of tumour development. *Math. Comput. Model.* **23**(6), 47–87.

[12] Chaplain, M.A.J., Lachowicz, M., Szymańska, Z., Wrzosek, D., 2011. Mathematical modelling of cancer invasion: The importance of cell-cell adhesion and cell-matrix adhesion. *Math Mod Meth Appl S* **21**, 719–743. doi:10.1142/S0218202511005192.

[13] Chauviere, A., Hillen, T., Preziosi, L., 2007. Modeling cell movement in anisotropic and heterogeneous network tissues. *Netw Heterog Media* **2**(2), 333–357.

[14] Cox, T.R., Erler, J.T., 2011. Remodeling and homeostasis of the extracellular matrix: implications for fibrotic diseases and cancer. *Disease Models and Mechanisms* **4**(2), 165–178.

[15] Domschke, P., Trucu, D., Gerisch, A., Chaplain, M., 2014. Mathematical modelling of cancer invasion: Implications of cell adhesion variability for tumour infiltrative growth patterns. *J. Theor. Biol.* **361**, 41–60.

[16] Gerisch, A., Chaplain, M., 2008. Mathematical modelling of cancer cell invasion of tissue: Local and non-local models and the effect of adhesion. *J. Theor. Biol.* **250**, 684–704.

[17] Hanahan, D., Weinberg, R.A., 2000. The hallmarks of cancer. *Cell* **100**, 57–70. doi:10.1016/S0092-8674(00)81683-9.

[18] Hanahan, D., Weinberg, R.A., 2011. The hallmarks of cancer: The next generation. *Cell* **144**, 646–674.

[19] Hillen, T., 2006. M5 mesoscopic and macroscopic models for mesenchymal motion. *Journal of Mathematical Biology* **53**(4), 585–616. doi:10.1007/s00285-006-0017-y.

[20] Hills, C.E., Younis, M.Y.G., Bennett, J., Siamantouras, E., Liu, K.K., Squires, P.E., 2012. Calcium-sensing receptor activation increases cell-cell adhesion and -cell function. *Cell Physiol Biochem* **30**(3), 575–586. doi:10.1159/000341439.

[21] Holle, A.W., Young, J.L., Spatz, J.P., 2016. In vitro cancer cell–ecm interactions inform in vivo cancer treatment. *Advanced Drug Delivery Reviews* **97**(Supplement C), 270–279. doi:10.1016/j.addr.2015.10.007.

[22] Katt, M.E., Placone, A.L., Wong, A.D., Xu, Z.S., Searson, P.C., 2016. In vitro tumor models: Advantages, disadvantages, variables, and selecting the right platform. *Frontiers in Bioengineering and Biotechnology* **4**(12).

[23] Lodish, H., Berk, A., Zipursky, S., 2000. Molecular Cell Biology. 4th ed., W.H.Freeman.

[24] Nabeshima, K., Inoue, T., Shimao, Y., Sameshima, T., 2002. Matrix metalloproteinases in tumor invasion: Role for cell migration. *Pathology International* **52**(4), 255–264.

[25] Painter, K.J., 2008. Modelling cell migration strategies in the extracellular matrix. *Journal of Mathematical Biology* **58**(4), 511. doi:10.1007/s00285-008-0217-8.

[26] Parsons, S.L., Watson, S.A., Brown, P.D., Collins, H.M., Steele, R.J., 1997. Matrix metalloproteinases. *Brit J Surg* **84**(2), 160–166. doi:10.1046/j.1365-2168.1997.02719.x.

[27] Peng, L., Trucu, D., Lin, P., Thompson, A., Chaplain, M.A.J., 2016. A multiscale mathematical model of tumour invasive growth. *Bull. Math. Biol.* doi:10.1007/s11538-016-0237-2.

[28] Ramis-Conde, I., Drasdo, D., Anderson, A.R., Chaplain, M.A., 2008. Modeling the influence of the e-cadherin-beta-catenin pathway in cancer cell invasion: a multiscale approach. *Biophys. J.* **95**(1), 155–165.

[29] Shah, D., Tseng, W., Martinez, S., 2012. Treatment options for metaplastic breast cancer. *ISRN Oncology* **2012**.

[30] Trucu, D., Lin, P., Chaplain, M.A.J., Wang, Y., 2013. A multiscale moving boundary model arising in cancer invasion. *Multiscale Model. Simul.* **11**(1), 309–335.

[31] Wang, Z., Hillen, T., Li, M., 2008. Mesenchymal motion models in one dimension. *SIAM J. Appl. Math.* **69**(2), 375–397.

[32] Weigelt, B., Peterse, J.L., van't Veer, L.J., 2005. Breast cancer metastasis: markers and models. *Nat Rev Cancer* **5**(8), 591–602.

[33] Wijnhoven, B., Dinjens, W., Pignatelli, M., 2000. E-cadherin-catenin cell-cell adhesion complex and human cancer. *Brit J Surg* **87**(8), 992–1005.

[34] Yamaguchi, H., Wyckoff, J., Condeelis, J., 2005. Cell migration in tumors. *Current Opinion in Cell Biology* **17**(5), 559–564. doi:10.1016/j.ceb.2005.08.002.

[35] Yang, H., 2012. Mathematical modelling of solid cancer growth with angiogenesis. *Theor. Biol. and Med. Mod.* **9**(2).